HHS Public Access

Author manuscript

J Neuroimmune Pharmacol. Author manuscript; available in PMC 2022 October 08.

Published in final edited form as:

J Neuroimmune Pharmacol. 2022 June ; 17(1-2): 181–194. doi:10.1007/s11481-021-09995-2.

HIV-1 gp120-induced endolysosome de-acidification leads to efflux of endolysosome iron, and increases in mitochondrial iron and reactive oxygen species

Peter W. Halcrow[#],
Department of Biomedical Sciences, University of North Dakota School of Medicine and Health Sciences, Grand Forks, ND 58203, USA

Koffi L. Lakpa[#],
Department of Biomedical Sciences, University of North Dakota School of Medicine and Health Sciences, Grand Forks, ND 58203, USA

Nabab Khan,
Department of Biomedical Sciences, University of North Dakota School of Medicine and Health Sciences, Grand Forks, ND 58203, USA

Zahra Afghah,
Department of Biomedical Sciences, University of North Dakota School of Medicine and Health Sciences, Grand Forks, ND 58203, USA

Nicole Miller,
Department of Biomedical Sciences, University of North Dakota School of Medicine and Health Sciences, Grand Forks, ND 58203, USA

Gaurav Datta,
Department of Biomedical Sciences, University of North Dakota School of Medicine and Health Sciences, Grand Forks, ND 58203, USA

Xuesong Chen,
Department of Biomedical Sciences, University of North Dakota School of Medicine and Health Sciences, Grand Forks, ND 58203, USA

Jonathan D. Geiger[*]

[*]Address correspondence to: Jonathan D. Geiger, Ph.D., Chester Fritz Distinguished Professor, Department of Biomedical Sciences, University of North Dakota School of Medicine and Health Sciences, 504 Hamline Street, Room #110, Grand Forks, North Dakota 58203, (701) 777-2183 (P), (701) 777-0387 (F), jonathan.geiger@und.edu.

[#]These authors contributed equally to this work

Author contributions statement: K.L.L wrote the manuscript, conducted and analyzed mitochondrial iron assays and formatted the figures and references. P.H. conducted initial experiments and analyzed data from assays of iron, pH, and ROS. N.K. helped with experimental design and conducted cytosolic and mitochondrial ROS assays. Z.A. conducted and analyzed mitochondrial iron assays in the absence and presence of inhibitors. N.M. analyzed mitochondrial experiment data blinded to experimental treatments. G.D. conducted experiments to determine effects of iron in the absence and presence of inhibitors on endolysosome morphology. X.C. helped with experimental design and editing of the manuscript. These studies were largely conceptualized by J.D.G. who was primarily responsible for editing the manuscript.

Conflict of interest/Competing Interest: The authors declare that this manuscript was written in the absence of any commercial or financial relationships that could be construed as a potential conflict of interest.

Availability of data and material: Not applicable

Code availability: Not applicable

Department of Biomedical Sciences, University of North Dakota School of Medicine and Health Sciences, Grand Forks, ND 58203, USA

Abstract

The HIV-1 coat protein gp120 continues to be implicated in the pathogenesis of HIV-1 associated neurocognitive disorder (HAND); a condition known to affect ~50% of people living with HIV-1 (PLWH). Autopsy brain tissues of HAND individuals display morphological changes to mitochondria and endolysosomes, and HIV-1 gp120 causes mitochondrial dysfunction including increased levels of reactive oxygen species (ROS) and de-acidification of endolysosomes. Ferrous iron is linked directly to ROS production, ferrous iron is contained in and released from endolysosomes, and PLWH have elevated iron and ROS levels. Based on those findings, we tested the hypothesis that HIV-1 gp120-induced endolysosome de-acidification and subsequent iron efflux from endolysosomes is responsible for increased levels of ROS. In U87MG glioblastoma cells, HIV-1 gp120 de-acidified endolysosomes, reduced endolysosome iron levels, increased levels of cytosolic and mitochondrial iron, and increased levels of cytosolic and mitochondrial ROS. These effects were all attenuated significantly by the endolysosome-specific iron chelator deferoxamine, by inhibitors of endolysosome-resident two-pore channels and divalent metal transporter-1 (DMT-1), and by inhibitors of mitochondria-resident DMT-1 and mitochondrial permeability transition pores. These results suggest that oxidative stress commonly observed with HIV-1 gp120 is downstream of its ability to de-acidify endolysosomes, to increase the release of iron from endolysosomes, and to increase the uptake of iron into mitochondria. Thus, endolysosomes might represent early and upstream targets for therapeutic strategies against HAND.

Keywords

HIV-1 gp120; endosomes; lysosomes; mitochondria; reactive oxygen species; iron; lysosomal stress response

Introduction

HIV-associated neurocognitive disorder (HAND) affects about 50% of people living with HIV-1 (PLWH) despite effective viral suppression achieved using antiretroviral therapeutics (ART) (McArthur et al., 2010). Clinically, HAND presents with deficits in cognition, memory, and motor function (Clifford and Ances, 2013); the severity varies from mild (asymptomatic) to severe (dementia) (Antinori et al., 2007). Pathologically, post-mortem brain samples exhibit decreased synaptodendritic arborization (Masliah et al., 1992; Masliah et al., 1997; Everall et al., 1999), Alzheimer's disease-like changes (Brew et al., 2005), and morphological changes in subcellular organelles including endolysosomes (Gelman et al., 2005), endoplasmic reticulum (Lindl et al., 2007), and mitochondria (Fields et al., 2013; Avdoshina et al., 2016). Implicated in the pathogenesis of HAND are HIV-1 proteins (Kovalevich and Langford, 2012), reactive oxygen species (ROS) (Turchan et al., 2003) as well as ART drugs used to treat PLWH (Heaton et al., 2011). However, the full spectrum of underlying mechanisms of HAND remains unclear.

Several soluble factors, including the HIV-1 proteins transactivator of transcription (Tat) and glycoprotein 120 (gp120) continue to be implicated in the pathogenesis of HAND (Kovalevich and Langford, 2012). Tat and gp120 are neurotoxic, decrease synaptodendritic arborization (Toggas et al., 1996; Fields et al., 2013; Fitting et al., 2013), and disrupt intracellular levels of calcium and iron (Nath et al., 1995; Haughey et al., 2001; Festa et al., 2015). Furthermore, Tat and gp120 are capable of affecting the structure and function of subcellular organelles including endolysosomes and mitochondria (Hui et al., 2012; Bae et al., 2014; Avdoshina et al., 2016; Fields et al., 2016; Datta et al., 2019).

Endosomes and lysosomes, collectively referred to here as endolysosomes, are dynamic organelles involved in the trafficking and degradation of intracellular cargo. Endolysosomes are acidic organelles that help regulate a wide variety of essential physiological functions including plasma membrane repair, cell homeostasis, energy metabolism, nutrient-dependent signal transduction, and immune responses (Jaiswal et al., 2002; Bird et al., 2009; Settembre et al., 2013; Mony et al., 2016; Ballabio and Bonifacino, 2020). Additionally, endolysosomes contain readily releasable stores of biologically important cations including calcium and iron (Xiong and Zhu, 2016). De-acidification of endolysosomes, such as has been shown to occur with Tat and gp120 (Pietrella et al., 1998; Hui et al., 2012; Bae et al., 2014), releases calcium and iron (Christensen et al., 2002; Fernández et al., 2016) from endolysosomes and disrupts endolysosome membrane integrity (Hui et al., 2015). These actions of Tat and gp120 might affect mitochondrial function because calcium and iron overload in mitochondria can result in increased levels of ROS and cell death via apoptosis and ferroptosis (Brookes et al., 2004; Dixon et al., 2012; Huang et al., 2017).

PLWH often exhibit elevated serum iron levels (Chang et al., 2015), and iron has been implicated in HIV-1 progression and HAND pathogenesis (Nekhai et al., 2013; Chang et al., 2015; Patton et al., 2017). Extracellular ferric iron (Fe^{3+}) binds to the iron transport protein transferrin and is endocytosed into endosomes where it is reduced to ferrous iron (Fe^{2+}). Endolysosomes play an essential role in maintaining intracellular levels of iron; these acidic organelles are known to release iron when they are de-acidified and they contain a variety of cation channels through which iron can be released into the cytosol (Kurz et al., 2011;Dong et al., 2008; Fernández et al., 2016). Through Fenton reactions (Eaton and Qian, 2002), ferrous iron in endolysosomes, cytoplasm, and mitochondria can generate ROS and can cause oxidative stress. Oxidative stress continues to be implicated in the pathogenesis of neurodegenerative diseases including HAND, and others and we have shown that Tat and gp120 both increase levels of ROS (Foga et al., 1997; Kim et al., 2015; Viviani et al., 2001). Furthermore, HIV-1 gp120 can damage subcellular organelles, such as endolysosomes and mitochondria (Viviani et al., 2001; Bae et al., 2014; Avdoshina et al., 2016; Fields et al., 2016). However, prior to this study nothing was known about the extent to which gp120-induced release of iron from endolysosomes led to increased levels of ROS in the cytosol and in mitochondria. Therefore, we tested the hypothesis that HIV-1 gp120-induced de-acidification of endolysosomes led to an efflux of iron from endolysosomes, an accumulation of iron in the cytosol and mitochondria, and subsequent increases in levels of cytosolic and mitochondrial ROS.

Materials and Methods

Cell cultures:

Glioblastoma (U87MG) cells were cultured in 1x DMEM (Invitrogen) containing 10% fetal bovine serum and 1% penicillin/streptomycin (Invitrogen). U87MG cells were grown in T75 flasks and then sub-cultured in 35 mm^2 dishes (Mattek) or 12-and 24-well plates (Corning); cells were maintained in a 5% CO_2 incubator at 37°C. Cells were not used past their tenth passage.

Propidium iodide cell death assay:

Cell death was measured by cellular uptake of propidium iodide (PI) staining (Sigma-Aldrich) (Crowley et al., 2016). U87MG cells were treated with gp120 (4 nM) in the absence or presence of deferoxamine (DFO; 100 μM) for 30 min or 24 h. Cells were washed once with pre-warmed 1x PBS then suspended in a PI (20 μg/mL) + PBS buffer for 30 min. Cells were analyzed using our Attune NxT flow cytometer. PI was excited by the blue (488 nm) excitation laser and light emission was determined using a BL2 (574/26 nm) filter. Mean fluorescent intensity, standard error of the mean, and the number (n) cells analyzed for PI were determined using Attune NxT software (ThermoFisher).

Endolysosome pH measurements:

As previously described (Hui et al., 2012), endolysosome pH was measured using a ratiometric indicator-dye LysoSensor Yellow/Blue DND-160; a dual excitation dye that measures pH independently of intracellular dye concentration. U87MG cells were loaded with 5 to 10 μM DND-160 for 5 min at 37°C. Post-incubation, dye-containing media was removed, and fresh media was added to the cells just prior to imaging. Light emitted at 520 nm in response to excitation for 2 msec at 340/380 nm was measured every 10 seconds using a filter-based imaging system (Zeiss Axiovert 200M, Germany). Ratios of light excited (340/380 nm) versus light emitted (520 nm) were converted to pH using a calibration curve as previously described (Hui et al., 2012). Using the formula $pH = -\log[H^+]$ we calculated percent reductions of intraluminal proton concentrations.

Endolysosome morphology:

Morphological features of plasma membranes, nucleus, and endolysosomes were determined by immunostaining. Lysosomes were stained with an anti-LAMP1 antibody and an Alexa 488 anti-rabbit secondary antibody. Plasma membranes were stained with an anti-beta1 sodium potassium ATPase antibody and an Alexa 594 anti-mouse antibody. Nuclei were stained with DAPI. Confocal scanning microscopy (Zeiss LSM800) was used to acquire z-stack images with a stack interval of 0.4 μm. Images were acquired and then reconstructed using Imaris (Oxford Instruments) imaging software (version 9.5).

Endolysosome iron measurements:

FeRhoNox-1 (Goryo Chemical), which stains specifically for Fe^{2+} (Hirayama, 2018), was added at a final concentration of 30 μM; U87MG cells were seeded at a density of $8x10^3$ cells on 35 mm^2 dishes and incubated at 37°C for 1 h. After washing cells twice with 1

x PBS, fresh PBS was added, and cells were imaged at an excitation wavelength of 537 nm and an emission wavelength of 569 nm using our confocal scanning microscope (Zeiss, LSM800). Imaging parameters were kept the same throughout each set of experiments. Z-stack images were taken at a stack interval of 0.4 μm. Images were reconstructed using Imaris (Oxford Instruments) imaging software (version 9.5). The data were represented as mean fluorescence intensity (MFI).

Cytosolic iron measurements:

Cytosolic iron levels were measured using PhenGreen™ SK diacetate (PGSK); a quenching probe for cytosolic iron (Petrat et al., 1999). U87MG cells were seeded at a density of 2 to 3 x 10^4 cells on 35 mm^2 dishes and incubated with PGSK at a final concentration of 10 μM for 30 min at 37°C. Cells were washed three-times with 1 x PBS, collected, suspended and analyzed using our Attune NxT flow cytometer (ThermoFisher). PGSK was excited using the blue (488 nm) excitation laser and light was captured after passing through the BL1 (530/30 nm) emission filter. Mean fluorescent intensities, standard error of the mean, and the numbers (n) of cells analyzed for PGSK were determined using Attune NxT software (ThermoFisher).

Mitochondrial iron measurements:

Mitochondrial iron levels were measured using rhodamine B-[2,2'-bipyridine-4-yl)-aminocarbonyl]benzyl ester (RDA) (Squarix). RDA is a Fe^{2+}-specific quenching dye that localizes within mitochondria; it excites at 562 nm and emits at 598 nm (Rauen et al., 2007). U87MG cells were seeded at a density of 2 to 3 x 10^4 cells on 35 mm^2 dishes and incubated with 200 nM RDA for 10 min at 37°C. Cells were washed once and resuspended with 1 x PBS. Z-stack images were captured using confocal scanning microscopy (Zeiss LSM800); 11 to 23 slices were used per z-stack image. Imaging parameters were kept the same throughout each set of experiments. Images were taken before and 30 min after the addition of HIV-1 gp120. In the deferoxamine (DFO) treatment group, cells were incubated with DFO for 1 h followed by the removal of DFO-containing media and the continuation of the above-described protocol. ImageJ software was used to merge z-stack images, and to measure mean fluorescence intensity (MFI) before (time zero) and after (time 30') the addition of HIV-1 gp120 or vehicle. MFI per cell was determined by dividing MFI values at time zero by MFI values at time 30' (ratio 0/30') and values were expressed as a percentage; the values were normalized to control values obtained with heat-inactivated HIV-1 gp120 ($gp120^i$).

ROS measurements in cytosol and mitochondria:

Cytosolic ROS levels were measured using 2,7-dichlorodihydrofluoroscein diacetate (DCFDA), which when oxidized produces DCF; DCF excites at 495 nm and emits at 529 nm. Mitochondrial ROS was measured using MitoSox Red Superoxide Indicator, which excites at 510 nm and emits at 580 nm. U87MG cells seeded at a density of 2 to 3 x 10^4 were incubated with 10 μM DCFDA or 5 μM MitoSox for 30 min at 37°C in serum-free media. Cells were then washed twice with 1 x PBS prior to being analyzed using our Attune NxT flow cytometer (ThermoFisher). DCF-stained cells were excited by the blue (488 nm) excitation laser and light was emitted through the BL1 (530/30 nm) emission filter. MitoSox

Red stained cells were excited by the blue (488 nm) excitation laser and light was emitted by the BL2 (574/26 nm) emission filter. Mean fluorescence intensities, standard error of the mean, and the number (n) of cells analyzed for DCF and MitoSox Red were determined using Attune NxT software (ThemoFisher).

Reagents:

Reagents were purchased from ThermoFisher Scientific unless noted otherwise; CISMBI (Sigma-Aldrich), TRO-19622 (TOCRIS) and Ned-19 (TOCRIS). HIV-1 gp120 IIIb was purchased from ABL Inc. and prepared aliquots were stored at −80°C to prevent freeze-thaw problems.

Statistics:

All data were expressed as means and standard errors of the mean (SEM). Data analyses were completed using GraphPad Prism 8 software. Statistical significance between two groups was determined using a Student's t test. One-way ANOVA with Tukey's post-hoc tests were used to compare differences between multiple groups. $p<0.05$ was designated to be statistically significant. All experiments were conducted a minimum of 3 independent times.

Results

HIV-1 gp120 and deferoxamine treatment did not affect cell viability:

The main focus of the studies reported here was to determine the effects of HIV-1 gp120 on intracellular levels of Fe^{2+} and links between Fe^{2+} and ROS; not gp120-induced cell death. Accordingly, we determined under our experimental conditions whether gp120 decreased cell viability (Dawson et al., 1993; Nath et al., 2000; Yang et al., 2010). Using propidium iodide (PI) uptake as a measure of cell death (Crowley et al., 2016), no statistically significant changes in PI mean fluorescence intensity (MFI) was observed between control and HIV-1 gp120 (4 nM) treatments for 30 min (Supplemental Figure 1A) or 24 h (Supplemental Figure 1B). We found also that treatments with the endolysosome iron chelator deferoxamine (DFO, 100 μM) for 30 min (Supplemental Figure 1A) or 24 h (Supplemental Figure 1B) did not affect cell viability in the absence or presence of gp120 (4 nM).

HIV-1 gp120 treatment increased endolysosome pH and volumes, and decreased endolysosome numbers:

Next, we determined the effect of HIV-1 gp120 treatment on endolysosome pH. HIV-1 gp120 (4 nM) resulted in endolysosome de-acidification (Figure 1A); peak deacidification was observed by 30 min and pH units were significantly ($p<0.0001$) increased by 0.13 ± 0.01 pH units from control values of 5.28 ± 0.01 to values of 5.41 ± 0.01 (Figure 1B). Bafilomycin A1 (Baf A1, 200 nM), a vacuolar ATPase inhibitor that de-acidifies endolysosomes (Yoshimori et al., 1991), was used as a positive control and it significantly ($p<0.0001$) increased endolysosome pH by 0.18 ± 0.01 pH units from control values of 5.28 ±0.01 to 5.46 ± 0.01 (Figure 1B). These changes in pH corresponded to a 32% reduction in intraluminal proton concentration by Baf A1 and a 25% reduction by HIV-1 gp120. The

endolysosome de-acidification by HIV-1 gp120 remained elevated for 30 min while the effects of Baf A1 normalized about 12 min following its application (Figure 1A).

These findings led us to check the effects of HIV-1 gp120 on endolysosome morphology. Endolysosome de-acidification has been shown by others and us to change endolysosome morphology including numbers, sizes and positioning within cells (Dong et al., 2010; Hui et al., 2012; Fernández et al., 2016; Johnson et al., 2016; Mauthe et al., 2018). Because HIV-1 gp120 de-acidified endolysosomes, we next determined the effects of HIV-1 gp120 on endolysosome numbers, sizes and cellular positioning. Qualitatively, endolysosomes exposed to heat-inactivated gp120 ($gp120^{i}$) displayed a perinuclear distribution pattern, but when exposed to HIV-1 gp120 endolysosomes were larger and more dispersed towards plasma membranes (Figure 1C). Quantitatively, HIV-1 gp120 significantly ($p<0.0001$) decreased the number of LAMP1-positive vesicles per cell from 371 ± 19 to 256 ± 34 (Figure 1D), but nevertheless increased significantly ($p<0.0001$) the total volume (μm^3) of LAMP1-positive vesicles by 47% (Figure 1E). Similarly, Baf A1 significantly ($p<0.0001$) decreased the number of LAMP1-positive vesicles from 371 ± 19 to 264 ± 19 (Figure 1D) and significantly ($p<0.0001$) increased the total volume of LAMP1-positive vesicles by 36% (Figure 1E).

HIV-1 gp120-induced decreases in levels of endolysosome iron were blocked by an inhibitor of two pore channels:

De-acidification of endolysosomes can induce the release of divalent cations from endolysosomes (Christensen et al., 2002)(Fernández et al., 2016). Because of this, we next determined the extent to which heat-inactivated HIV-1 gp120 ($gp120^{i}$), HIV-1 gp120 (gp120), and bafilomycin A1 (Baf) affected levels of endolysosome iron. Qualitatively, treatment of U87MG cells for 30 min with 4 nM HIV-1 gp120 (Figure 2B) but not $gp120^{i}$ (Figure 2A) decreased FeRhoNox-1 fluorescence staining for Fe^{2+}. Quantitatively, HIV-1 gp120 decreased significantly ($p<0.01$) levels of endolysosome iron by 41% (Figure 2C); the positive control bafilomycin A1 decreased significantly ($p<0.0001$) levels of endolysosome iron by 66% and this decrease was significantly ($p<0.01$) greater than that produced by gp120 (Figure 2C).

We next investigated the extent to which the release of endolysosome Fe^{2+} induced by HIV-1 gp120 involved endolysosome-resident two-pore channels (TPCs) in part because TPCs are localized on endolysosomes and because they are permeable to divalent cations such as Fe^{2+} (Brailoiu et al., 2009; Calcraft et al., 2009; Fernández et al., 2016).
As expected, we observed a robust co-localization between FeRhoNox-1 and LAMP1 staining regardless of the treatments applied (Supplemental Figure 2A–D). Qualitatively, HIV-1 gp120 decreased FeRhoNox-1 staining in endolysosomes and these decreases were blocked by the TPC inhibitor Ned-19 (Supplemental Figure 2A–D). Compared to control treatments with heat-inactivated HIV-1 $gp120^{i}$ (Figure 2A), HIV-1 gp120 (4 nM) decreased significantly ($p<0.01$) levels of endolysosome iron (Figure 2C) and caused marked changes in endolysosome morphology (Figure 2B); these effects of HIV-1 gp120 were significantly ($p<0.01$) blocked by pretreatment of cells with NED-19, an antagonist of TPC (Figure 2D).

HIV-1 gp120-induced increases in cytosolic iron and ROS were blocked by chelation of endolysosome iron, and inhibitors of two-pore channels (TPCs) and divalent metal transporter 1 (DMT1):

Having found that HIV-1 gp120 caused increased release of Fe^{2+} from endolysosomes, we next sought to determine the extent to which and mechanisms by which HIV-1 gp120 affected levels of cytosolic Fe^{2+} and levels of cytosolic ROS. Cytosolic Fe^{2+} levels were measured with the quenching metal indicator PhenGreen SK (PGSK) (Petrat et al., 1999). HIV-1 gp120 (4 nM) significantly ($p<0.0001$) increased levels of cytosolic Fe^{2+} by about 40% (Figure 3A). Pretreatment with 100 μM deferoxamine (DFO), a specific chelator of endolysosome Fe^{2+}, significantly ($p<0.0001$) blocked HIV-1 gp120-induced increases in cytosolic Fe^{2+} (Figure 3A). Because levels of ROS are increased by Fe^{2+} through Fenton-reaction chemistry, we determined the extent to which endolysosome iron released by HIV-1 gp120 affected cytosolic ROS levels. HIV-1 gp120 (4 nM) increased significantly ($p<0.0001$) by about 66% levels of cytosolic ROS (Figure 3B). By itself, DFO (100 μM) significantly ($p<0.0001$) inhibited cytosolic levels of ROS and DFO significantly ($p<0.0001$) blocked HIV-1 gp120-induced increases in cytosolic ROS (Figure 3B). Based on these findings as well as findings described above, we investigated next the effects of blocking HIV-1 gp120-induced endolysosome iron release through two-pore channels on cytosolic ROS levels. Pretreatment of cells for 30 min with the TPC inhibitor Ned-19 (10 μM) significantly ($p<0.05$) blocked HIV-1 gp120-induced increases in ROS (Figure 3C). Because Fe^{2+} in endolysosomes can also be released through divalent metal transporter 1 (DMT1), we next determined the extent to which the DMT1 inhibitor CISMBI affected HIV-1 gp120-ineuced increases in cytosolic ROS and found that CISMBI significantly ($p<0.01$) blocked HIV-1 gp120-induced increases in ROS (Figure 3D).

HIV-1 gp120-induced increases in mitochondrial iron and ROS were reduced by chelation of endolysosome iron and by inhibitors of two-pore channels, divalent metal transporter 1, and mitochondrial permeability transition pore:

Mitochondria uptake cytosolic Fe^{2+} and we determined next the extent to which HIV-1 gp120-induced release of endolysosome Fe^{2+} resulted in increased levels of Fe^{2+} in mitochondria using the “turn-off” quenching dye rhodamine B-[(2,2’-bipyridine-4-yl)-aminocarbonyl]benzyl ester (RDA) and increased levels of mitochondrial ROS using MitoSox Red. Qualitatively, increased levels of mitochondrial Fe^{2+} were observed in cells treated with HIV-1 gp120, but not with heat-inactivated $gp120^{i}$, DFO, or DFO added prior to HIV-1 gp120 (Supplemental Figure 3A). Quantitatively, HIV-1 gp120 (4 nM) significantly ($p<0.0001$) increased levels of mitochondrial Fe^{2+} (decreased RDA MFI) by, on average, about 28% (Figure 4A). Pre-treatment of cells with DFO (100 μM) prior to the addition of HIV-1 gp120 significantly ($p<0.0001$) blocked HIV-1 gp120-induced increases in mitochondrial Fe^{2+} (Figure 4A). Because levels of ROS are increased by Fe^{2+} through Fenton-reaction chemistry, we determined next the extent to which endolysosome iron released by HIV-1 gp120 affected mitochondrial ROS levels. HIV-1 gp120 (4 nM) increased significantly ($p<0.0001$), by about 89%, levels of mitochondrial ROS (Figure 4B). DFO (100 μM) alone did not affect levels of mitochondrial ROS but did significantly ($p<0.001$) block gp120-induced increases in mitochondrial ROS (Figure 4B).

Mechanistically, we next determined the extent to which inhibitors of mitochondrial permeability transition pores (mPTP), DMT1, and endolysosome TPCs could block HIV-1 gp120-induced increases in levels of mitochondrial Fe^{2+}. Qualitatively, increased levels of mitochondrial iron were observed in cells treated with HIV-1 gp120; these increases were blocked by the mPTP inhibitor TRO-19622 (TRO), the DMT1 competitive inhibitor 2-(3-carbamimidoylsulfanylmethyl-benzyl)-isothiourea (CISMBI) (Montalbetti et al., 2014), and the TPC inhibitor trans-Ned-19 (Ned-19) (Supplemental Figure 3B). Quantitatively, HIV-1 gp120 (4 nM) significantly ($p<0.0001$) increased levels of mitochondrial iron (Figure 4C) and these increases were blocked by pre-treating cells for 30 min with 3 μM of TRO ($p<0.0001$), 100 μM of CISMBI ($p<0.001$), or 10 μM of Ned-19 (Figure 4C). In terms of ROS levels, pretreatment of cells for 30 min with Ned-19 (10 μM), TRO (3 μM) and CISMBI (100 μM) all significantly ($p<0.0001$) reduced HIV-1 gp120-induced increases in mitochondrial ROS (Figure 4D–F).

Discussion

Over the past three decades, the development and use of effective antiretroviral therapeutics (ART) has transformed HIV-1/AIDS into a chronic therapeutically managed disease (Arts and Hazuda, 2012). Associated with HIV-1/AIDS in the ART-era is a high prevalence of a spectrum of cognitive, motor and behavioral symptoms ranging in intensity from mild (asymptomatic) to severe (dementia) (McArthur et al., 2010). Collectively, these symptoms are referred to as HIV-1 associated neurocognitive disorders (HAND) (Antinori et al., 2007; Clifford and Ances, 2013) and underlying its pathology are findings of increased levels of oxidative stress, subcellular organelle dysfunction, synaptodendritic damage, and neuroinflammation (Everall et al., 1999; Gelman et al., 2005; Kovalevich and Langford, 2012; Avdoshina et al., 2016; Fields et al., 2016; Saylor et al., 2016; Sanchez and Kaul, 2017; Scutari et al., 2017). Implicated in the pathogenesis of HAND are soluble factors including the HIV-1 proteins Tat and gp120 as well as ART treatments themselves (Sanchez and Kaul, 2017; Scutari et al., 2017). Accordingly, additional investigative work is required to understand better the mechanisms underlying HAND pathogenesis with the goal of identifying effective therapeutic interventions.

Here, we showed that HIV-1 gp120 de-acidified endolysosomes, increased the release of ferrous iron out of endolysosomes, and that this released iron accumulated in the cytosol and mitochondria where it increased levels of ROS. Furthermore, we showed the involvement of two pore channels, divalent metal transporter 1, and mitochondrial permeability transport pore opening in these effects. By inhibiting iron release from endolysosomes and/or iron uptake into mitochondria it was possible to block HIV-1 gp120-induced effects on iron homeostasis and ROS production. Together these results suggest that HIV-1 gp120-induced changes to mitochondria might be downstream of endolysosome effects and that therapeutic strategies against HAND might be directed against these upstream targets (Figure 5).

Previously, we reported that HIV-1 gp120 de-acidified neuronal endolysosomes and that this de-acidification was reversed by the TRPML1 agonist ML-SA1 (Bae et al., 2014). Others too have reported, this time using human monocytes, that HIV-1 gp120 impaired endolysosome acidification (Pietrella et al., 1998). Here, we confirmed and extended

these studies by showing in U87MG glioblastoma cells that HIV-1 gp120 de-acidified endolysosome pH to an extent similar to the vacuolar ATPase inhibitor Baf A1; a known endolysosome de-acidifier (Yoshimori et al., 1991). Linked to endolysosome de-acidification are changes to endolysosome morphology including increased endolysosome volumes, decreased numbers of endolysosomes, and re-positioning of endolysosomes in cells (Ohkuma and Poole, 1981; Myers et al., 1991; Fernández et al., 2016; Datta et al., 2019). Accordingly, we determined the effects of HIV-1 gp120 on endolysosome volumes and numbers and found that HIV-1 gp120, similar to Baf A1, increased endolysosome volumes and decreased endolysosome numbers.

Endolysosome positioning inside of cells is influenced by multiple factors including nutrient status, motor proteins, and cytosolic and intra-lysosomal pH (Heuser, 1989; Parton et al., 1991; Korolchuk et al., 2011; Johnson et al., 2016; Pu et al., 2016). Previously, we reported that HIV-1 gp120 promoted the movement of endolysosomes away from the nucleus and towards plasma membranes as well as increased endolysosome exocytosis (Datta et al., 2019) and here using U87MG cells we found similarly that HIV-1 gp120 and the positive control Baf A1 both caused movement of endolysosomes towards the periphery of cells and away from their normal more perinuclear localization. We interpret our results that de-acidified endolysosomes localize towards the periphery of the cell while more acidic endolysosomes are positioned in a more juxtanuclear manner to support findings from multiple laboratories (Heuser, 1989; Parton et al., 1991; Johnson et al., 2016).

Endolysosomes contain multiple mechanisms capable of regulating H^+ levels as well as levels of divalent cations including calcium, iron, copper and zinc (Abouhamed et al., 2006; Dong et al., 2008; Fernández et al., 2016), and endolysosome de-acidification is known to induce the release of these cations through various channels and transporters (Christensen et al., 2002; Fernández et al., 2016). Here we focused largely on two-pore channels (TPC) because of findings that they are endolysosome-resident and when activated by their endogenous agonist nicotinic adenine dinucleotide phosphate (NAADP) they release into the cytosol both calcium (Calcraft et al., 2009) and iron (Fernández et al., 2016). We found that HIV-1 gp120 significantly decreased levels of ferrous iron in endolysosomes and that HIV-1 gp120 significantly increased levels of ferrous iron in cytosol and mitochondria. Those findings suggested that HIV-1 gp120-induced release of ferrous iron from endolysosome stores were sufficient to increase levels in the cytosol and in mitochondria, and this suggestion was supported by findings that pretreatment with deferoxamine, an endocytosed cell-impermeable iron chelator that specifically chelates iron in endolysosomes (Lloyd et al., 1991; Cable and Lloyd, 1999), blocked the HIV-1 gp120-induced increases in the cytosol and mitochondria. Further, inhibiting mitochondrial permeability transition pore (mPTP) opening and divalent metal transporter 1 (DMT1) both blocked HIV-1 gp120-induced increases in mitochondrial iron. Because DMT1 are localized on mitochondria and endolysosome membranes (Abouhamed et al., 2006; Wolff et al., 2014; Wolff et al., 2018), our results with the DMT1 inhibitor CISMBI might have been the result of inhibiting endolysosome iron release and/or blocking mitochondrial iron uptake.

Although, our results suggest that HIV-1 gp120 disrupts endolysosome-mitochondrial iron signaling it is not yet clear how iron is transferred between the two organelles. One

possibility is a “kiss-and-run” mechanism where endolysosomes dock with and transfer iron to mitochondria (Das et al., 2016; Hamdi et al., 2016). Alternatively, endolysosome de-acidification might increase the iron translocation between endolysosomes and mitochondria and thereby contribute to oxidative stress (Uchiyama et al., 2008). Regardless, HIV-1 gp120-induced endolysosome iron efflux appears to be an upstream regulator of cytosolic and mitochondrial iron homeostasis.

A well-known biological consequence of elevated cytosolic and mitochondrial iron is the production of ROS through Fenton-based chemical reactions. We used assays to determine effects of HIV-1 gp120 on levels of intracellular hydroxyl radicals (·OH), hydrogen peroxide (H_2O_2), and superoxide radicals ($\cdot O_2^-$) as well as mitochondrial $\cdot O_2^-$ (Dikalov and Harrison, 2014). Our findings of HIV-1 gp120-induced increases in mitochondrial-generated superoxide and cytosolic ROS are consistent with previous findings that gp120 increased levels of intracellular ROS (Russo et al., 2005; Shah et al., 2013; Lopez et al., 2017; Datta et al., 2019). Our findings that pre-treatment with DFO reduced significantly HIV-1 gp120-induced increases in ROS strongly suggest the involvement of endolysosome iron in these effects, but we cannot rule out the possibility that other cations might also be involved as well as the possible involvement of endolysosome-independent mechanisms. Although another study showed that endolysosome de-acidification led to increased ROS in mitochondria independent of endolysosome iron release (Yambire et al., 2019) it is possible that their experimental paradigm of persistent de-acidification resulted in endolysosome iron depletion as well as sequestration of cytosolic iron by iron storage proteins.

Elevated levels of oxidative stress can result in many biological events up to and including cell death. Under the conditions used here, we did not find any significant increase in levels of cell death with 30 min or 24 h treatments with HIV-1 gp120, however others noted < 10% cell death in U87MG and SHSY5Y cells treated for 24 h with HIV-1 gp120 (Russo et al., 2005; Lopez et al., 2017). In contrast, 7 to 10 day treatments of U87MG cells increased cell viability and cell proliferation (Valentín-Guillama et al., 2018). Furthermore, HIV-1 gp120-induced increases in ROS promoted U87MG cell proliferation through the activation of glycolysis and the induction of protectant GRP78 (Lopez et al., 2017; Valentín-Guillama et al., 2018). Cancer cells have elevated ROS and antioxidant levels compared to non-cancer cells (Liou and Storz, 2010; Schieber and Chandel, 2014) and further studies are warranted to determine mechanisms underlying HIV-1 gp120-induced effects on cell proliferation, antioxidant levels, and cell viability.

Overall, our studies suggest that HIV-1 gp120 can induce a lysosomal stress response that includes the release of endolysosome stores of ferrous iron. Further, this release of iron from endolysosomes results in increased levels of iron in cytosol and mitochondria that results in increased oxidative stress. Thus, crosstalk between endolysosomes and mitochondria might participate in the pathogenesis of HAND and endolysosome iron might be targeted as an early and upstream target for therapeutic interventions against HAND.

Supplementary Material

Refer to Web version on PubMed Central for supplementary material.

Funding:

We gratefully acknowledge research support from the National Institute of General Medical Sciences under award numbers P30GM100329 and U54GM115458, the National Institute of Mental Health under award numbers R01MH100972, R01MH105329 and R01MH119000, the National Institute of Neurological Diseases and Stroke (NINDS) under award number R01NS065957, and the National Institute of Drug Abuse under award number R01DA032444. The authors would like to thank Parinaz Ghanbari for her expert help in illustrating Figure 5.

We gratefully acknowledge research support from the National Institute of General Medical Sciences under award numbers P30GM100329 and U54GM115458, the National Institute of Mental Health under award numbers R01MH100972, R01MH105329 and R01MH119000, the National Institute of Neurological Diseases and Stroke (NINDS) under award number R01NS065957, and the National Institute of Drug Abuse under award number R01DA032444. The authors would like to thank Parinaz Ghanbari for her expert help in illustrating Figure 5.

References

Abouhamed M, Gburek J, Liu W, Torchalski B, Wilhelm A, Wolff NA, Christensen EI, Thevenod F, Smith CP (2006) Divalent metal transporter 1 in the kidney proximal tubule is expressed in late endosomes/lysosomal membranes: implications for renal handling of protein-metal complexes. Am J Physiol Renal Physiol 290:F1525–1533. [PubMed: 16449358]

Antinori A et al. (2007) Updated research nosology for HIV-associated neurocognitive disorders. Neurology 69:1789–1799. [PubMed: 17914061]

Arts EJ, Hazuda DJ (2012) HIV-1 antiretroviral drug therapy. Cold Spring Harb Perspect Med 2:a007161. [PubMed: 22474613]

Avdoshina V, Fields JA, Castellano P, Dedoni S, Palchik G, Trejo M, Adame A, Rockenstein E, Eugenin E, Masliah E, Mocchetti I (2016) The HIV Protein gp120 Alters Mitochondrial Dynamics in Neurons. Neurotox Res 29:583–593. [PubMed: 26936603]

Bae M, Patel N, Xu H, Lee M, Tominaga-Yamanaka K, Nath A, Geiger J, Gorospe M, Mattson MP, Haughey NJ (2014) Activation of TRPML1 clears intraneuronal Abeta in preclinical models of HIV infection. The Journal of neuroscience : the official journal of the Society for Neuroscience 34:11485–11503. [PubMed: 25143627]

Ballabio A, Bonifacino JS (2020) Lysosomes as dynamic regulators of cell and organismal homeostasis. Nat Rev Mol Cell Biol 21:101–118. [PubMed: 31768005]

Bird PI, Trapani JA, Villadangos JA (2009) Endolysosomal proteases and their inhibitors in immunity. Nat Rev Immunol 9:871–882. [PubMed: 19935806]

Brailoiu E, Churamani D, Cai X, Schrlau MG, Brailoiu GC, Gao X, Hooper R, Boulware MJ, Dun NJ, Marchant JS, Patel S (2009) Essential requirement for two-pore channel 1 in NAADP-mediated calcium signaling. J Cell Biol 186:201–209. [PubMed: 19620632]

Brew BJ, Pemberton L, Blennow K, Wallin A, Hagberg L (2005) CSF amyloid beta42 and tau levels correlate with AIDS dementia complex. Neurology 65:1490–1492. [PubMed: 16275845]

Brookes PS, Yoon Y, Robotham JL, Anders MW, Sheu SS (2004) Calcium, ATP, and ROS: a mitochondrial love-hate triangle. Am J Physiol Cell Physiol 287:C817–833. [PubMed: 15355853]

Cable H, Lloyd JB (1999) Cellular uptake and release of two contrasting iron chelators. J Pharm Pharmacol 51:131–134. [PubMed: 10217310]

Calcraft PJ et al. (2009) NAADP mobilizes calcium from acidic organelles through two-pore channels. Nature 459:596–600. [PubMed: 19387438]

Chang HC, Bayeva M, Taiwo B, Palella FJ Jr., Hope TJ, Ardehali H (2015) Short communication: high cellular iron levels are associated with increased HIV infection and replication. AIDS Res Hum Retroviruses 31:305–312. [PubMed: 25291189]

Christensen KA, Myers JT, Swanson JA (2002) pH-dependent regulation of lysosomal calcium in macrophages. J Cell Sci 115:599–607. [PubMed: 11861766]

Clifford DB, Ances BM (2013) HIV-Associated Neurocognitive Disorder (HAND). Lancet Infect Dis 13:976–986. [PubMed: 24156898]

Crowley LC, Scott AP, Marfell BJ, Boughaba JA, Chojnowski G, Waterhouse NJ (2016) Measuring Cell Death by Propidium Iodide Uptake and Flow Cytometry. Cold Spring Harb Protoc 2016.

Das A, Nag S, Mason AB, Barroso MM (2016) Endosome-mitochondria interactions are modulated by iron release from transferrin. J Cell Biol 214:831–845. [PubMed: 27646275]

Datta G, Miller NM, Afghah Z, Geiger JD, Chen X (2019) HIV-1 gp120 Promotes Lysosomal Exocytosis in Human Schwann Cells. Front Cell Neurosci 13:329. [PubMed: 31379513]

Dawson VL, Dawson TM, Uhl GR, Snyder SH (1993) Human immunodeficiency virus type 1 coat protein neurotoxicity mediated by nitric oxide in primary cortical cultures. Proc Natl Acad Sci U S A 90:3256–3259. [PubMed: 8097316]

Diebold L, Chandel NS (2016) Mitochondrial ROS regulation of proliferating cells. Free Radic Biol Med 100:86–93. [PubMed: 27154978]

Dikalov SI, Harrison DG (2014) Methods for detection of mitochondrial and cellular reactive oxygen species. Antioxid Redox Signal 20:372–382. [PubMed: 22978713]

Dixon SJ, Lemberg KM, Lamprecht MR, Skouta R, Zaitsev EM, Gleason CE, Patel DN, Bauer AJ, Cantley AM, Yang WS, Morrison B 3rd, Stockwell BR (2012) Ferroptosis: an iron-dependent form of nonapoptotic cell death. Cell 149:1060–1072. [PubMed: 22632970]

Dong XP, Cheng X, Mills E, Delling M, Wang F, Kurz T, Xu H (2008) The type IV mucolipidosis-associated protein TRPML1 is an endolysosomal iron release channel. Nature 455:992–996. [PubMed: 18794901]

Dong XP, Shen D, Wang X, Dawson T, Li X, Zhang Q, Cheng X, Zhang Y, Weisman LS, Delling M, Xu H (2010) PI(3,5)P(2) controls membrane trafficking by direct activation of mucolipin Ca(2+) release channels in the endolysosome. Nat Commun 1:38. [PubMed: 20802798]

Eaton JW, Qian M (2002) Molecular bases of cellular iron toxicity. Free Radic Biol Med 32:833–840. [PubMed: 11978485]

Everall IP, Heaton RK, Marcotte TD, Ellis RJ, McCutchan JA, Atkinson JH, Grant I, Mallory M, Masliah E (1999) Cortical synaptic density is reduced in mild to moderate human immunodeficiency virus neurocognitive disorder. HNRC Group. HIV Neurobehavioral Research Center. Brain pathology (Zurich, Switzerland) 9:209–217. [PubMed: 10219738]

Fernández B, Fdez E, Gómez-Suaga P, Gil F, Molina-Villalba I, Ferrer I, Patel S, Churchill GC, Hilfiker S (2016) Iron overload causes endolysosomal deficits modulated by NAADP-regulated 2-pore channels and RAB7A. In: Autophagy, pp 1487–1506. [PubMed: 27383256]

Festa L, Gutoskey CJ, Graziano A, Waterhouse BD, Meucci O (2015) Induction of Interleukin-1beta by Human Immunodeficiency Virus-1 Viral Proteins Leads to Increased Levels of Neuronal Ferritin Heavy Chain, Synaptic Injury, and Deficits in Flexible Attention. The Journal of neuroscience : the official journal of the Society for Neuroscience 35:10550–10561. [PubMed: 26203149]

Fields J, Dumaop W, Rockenstein E, Mante M, Spencer B, Grant I, Ellis R, Letendre S, Patrick C, Adame A, Masliah E (2013) Age-dependent molecular alterations in the autophagy pathway in HIVE patients and in a gp120 tg mouse model: reversal with beclin-1 gene transfer. J Neurovirol 19:89–101. [PubMed: 23341224]

Fields JA, Serger E, Campos S, Divakaruni AS, Kim C, Smith K, Trejo M, Adame A, Spencer B, Rockenstein E, Murphy AN, Ellis RJ, Letendre S, Grant I, Masliah E (2016) HIV alters neuronal mitochondrial fission/fusion in the brain during HIV-associated neurocognitive disorders. Neurobiol Dis 86:154–169. [PubMed: 26611103]

Fitting S, Ignatowska-Jankowska BM, Bull C, Skoff RP, Lichtman AH, Wise LE, Fox MA, Su J, Medina AE, Krahe TE, Knapp PE, Guido W, Hauser KF (2013) Synaptic dysfunction in the hippocampus accompanies learning and memory deficits in human immunodeficiency virus type-1 Tat transgenic mice. Biol Psychiatry 73:443–453. [PubMed: 23218253]

Foga IO, Nath A, Hasinoff BB, Geiger JD (1997) Antioxidants and dipyridamole inhibit HIV-1 gp120-induced free radical-based oxidative damage to human monocytoid cells. Journal of acquired immune deficiency syndromes and human retrovirology : official publication of theInternational Retrovirology Association 16:223–229.

Gelman BB, Soukup VM, Holzer CE 3rd, Fabian RH, Schuenke KW, Keherly MJ, Richey FJ, Lahart (2005) Potential role for white matter lysosome expansion in HIV-associated dementia. J Acquir Immune Defic Syndr 39:422–425. [PubMed: 16010164]

Hamdi A, Roshan TM, Kahawita TM, Mason AB, Sheftel AD, Ponka P (2016) Erythroid cell mitochondria receive endosomal iron by a “kiss-and-run” mechanism. Biochim Biophys Acta 1863:2859–2867. [PubMed: 27627839]

Haughey NJ, Nath A, Mattson MP, Slevin JT, Geiger JD (2001) HIV-1 Tat through phosphorylation of NMDA receptors potentiates glutamate excitotoxicity. J Neurochem 78:457–467. [PubMed: 11483648]

Heaton RK et al. (2011) HIV-associated neurocognitive disorders before and during the era of combination antiretroviral therapy: differences in rates, nature, and predictors. J Neurovirol 17:3–16. [PubMed: 21174240]

Heuser J (1989) Changes in lysosome shape and distribution correlated with changes in cytoplasmic pH. J Cell Biol 108:855–864. [PubMed: 2921284]

Hirayama T (2018) Development of Chemical Tools for Imaging of Fe Ions in Living Cells: A Review. Acta Histochem Cytochem 51:137–143. [PubMed: 30510327]

Huang H, Chen J, Lu H, Zhou M, Chai Z, Hu Y (2017) Iron-induced generation of mitochondrial ROS depends on AMPK activity. Biometals 30:623–628. [PubMed: 28608291]

Hui L, Chen X, Haughey NJ, Geiger JD (2012) Role of endolysosomes in HIV-1 Tat-induced neurotoxicity. ASN Neuro 4:243–252. [PubMed: 22591512]

Hui L, Geiger NH, Bloor-Young D, Churchill GC, Geiger JD, Chen X (2015) Release of calcium from endolysosomes increases calcium influx through N-type calcium channels: Evidence for acidic store-operated calcium entry in neurons. Cell Calcium 58:617–627. [PubMed: 26475051]

Jaiswal JK, Andrews NW, Simon SM (2002) Membrane proximal lysosomes are the major vesicles responsible for calcium-dependent exocytosis in nonsecretory cells. J Cell Biol 159:625–635. [PubMed: 12438417]

Johnson DE, Ostrowski P, Jaumouille V, Grinstein S (2016) The position of lysosomes within the cell determines their luminal pH. J Cell Biol 212:677–692. [PubMed: 26975849]

Kim SH, Smith AJ, Tan J, Shytle RD, Giunta B (2015) MSM ameliorates HIV-1 Tat induced neuronal oxidative stress via rebalance of the glutathione cycle. Am J Transl Res 7:328–338. [PubMed: 25893035]

Koerver L, Papadopoulos C, Liu B, Kravic B, Rota G, Brecht L, Veenendaal T, Polajnar M, Bluemke A, Ehrmann M, Klumperman J, Jaattela M, Behrends C, Meyer H (2019) The ubiquitin-conjugating enzyme UBE2QL1 coordinates lysophagy in response to endolysosomal damage. EMBO Rep 20:e48014. [PubMed: 31432621]

Korolchuk VI, Saiki S, Lichtenberg M, Siddiqi FH, Roberts EA, Imarisio S, Jahreiss L, Sarkar S, Futter M, Menzies FM, O’Kane CJ, Deretic V, Rubinsztein DC (2011) Lysosomal positioning coordinates cellular nutrient responses. Nat Cell Biol 13:453–460. [PubMed: 21394080]

Kovalevich J, Langford D (2012) Neuronal toxicity in HIV CNS disease. Future Virol 7:687–698. [PubMed: 23616788]

Kurz T, Eaton JW, Brunk UT (2011) The role of lysosomes in iron metabolism and recycling. Int J Biochem Cell Biol 43:1686–1697. [PubMed: 21907822]

Lindl KA, Akay C, Wang Y, White MG, Jordan-Sciutto KL (2007) Expression of the endoplasmic reticulum stress response marker, BiP, in the central nervous system of HIV-positive individuals. Neuropathology and applied neurobiology 33:658–669. [PubMed: 17931354]

Lloyd JB, Cable H, Rice-Evans C (1991) Evidence that desferrioxamine cannot enter cells by passive diffusion. Biochem Pharmacol 41:1361–1363. [PubMed: 2018567]

Lopez SN, Rodriguez-Valentin M, Rivera M, Rodriguez M, Babu M, Cubano LA, Xiong H, Wang G, Kucheryavykh L, Boukli NM (2017) HIV-1 Gp120 clade B/C induces a GRP78 driven cytoprotective mechanism in astrocytoma. Oncotarget 8:68415–68438. [PubMed: 28978127]

Masliah E, Achim CL, Ge N, DeTeresa R, Terry RD, Wiley CA (1992) Spectrum of human immunodeficiency virus-associated neocortical damage. Ann Neurol 32:321–329. [PubMed: 1416802]

Masliah E, Heaton RK, Marcotte TD, Ellis RJ, Wiley CA, Mallory M, Achim CL, McCutchan JA, Nelson JA, Atkinson JH, Grant I (1997) Dendritic injury is a pathological substrate for human immunodeficiency virus-related cognitive disorders. HNRC Group. The HIV Neurobehavioral Research Center. Ann Neurol 42:963–972. [PubMed: 9403489]

Mauthe M, Orhon I, Rocchi C, Zhou X, Luhr M, Hijlkema KJ, Coppes RP, Engedal N, Mari M, Reggiori F (2018) Chloroquine inhibits autophagic flux by decreasing autophagosome-lysosome fusion. Autophagy 14:1435–1455. [PubMed: 29940786]

McArthur JC, Steiner J, Sacktor N, Nath A (2010) Human immunodeficiency virus-associated neurocognitive disorders: Mind the gap. Ann Neurol 67:699–714. [PubMed: 20517932]

Mony VK, Benjamin S, O'Rourke EJ (2016) A lysosome-centered view of nutrient homeostasis. Autophagy 12:619–631. [PubMed: 27050453]

Myers BM, Prendergast FG, Holman R, Kuntz SM, LaRusso NF (1991) Alterations in the structure, physicochemical properties, and pH of hepatocyte lysosomes in experimental iron overload. J Clin Invest 88:1207–1215. [PubMed: 1918375]

Nath A, Padua RA, Geiger JD (1995) HIV-1 coat protein gp120-induced increases in levels of intrasynaptosomal calcium. Brain Res 678:200–206. [PubMed: 7620888]

Nath A, Haughey NJ, Jones M, Anderson C, Bell JE, Geiger JD (2000) Synergistic neurotoxicity by human immunodeficiency virus proteins Tat and gp120: protection by memantine. Ann Neurol 47:186–194. [PubMed: 10665489]

Nekhai S, Kumari N, Dhawan S (2013) Role of cellular iron and oxygen in the regulation of HIV-1 infection. Future Virol 8:301–311. [PubMed: 23678366]

Ohkuma S, Poole B (1981) Cytoplasmic vacuolation of mouse peritoneal macrophages and the uptake into lysosomes of weakly basic substances. J Cell Biol 90:656–664. [PubMed: 7287819]

Parton RG, Dotti CG, Bacallao R, Kurtz I, Simons K, Prydz K (1991) pH-induced microtubule-dependent redistribution of late endosomes in neuronal and epithelial cells. J Cell Biol 113:261–274. [PubMed: 2010463]

Patton SM, Wang Q, Hulgan T, Connor JR, Jia P, Zhao Z, Letendre SL, Ellis RJ, Bush WS, Samuels DC, Franklin DR, Kaur H, Iudicello J, Grant I, Kallianpur AR (2017) Cerebrospinal fluid (CSF) biomarkers of iron status are associated with CSF viral load, antiretroviral therapy, and demographic factors in HIV-infected adults. Fluids Barriers CNS 14:11. [PubMed: 28427421]

Petrat F, Rauen U, de Groot H (1999) Determination of the chelatable iron pool of isolated rat hepatocytes by digital fluorescence microscopy using the fluorescent probe, phen green SK. Hepatology 29:1171–1179. [PubMed: 10094962]

Pietrella D, Monari C, Retini C, Palazzetti B, Bistoni F, Vecchiarelli A (1998) Human immunodeficiency virus type 1 envelope protein gp120 impairs intracellular antifungal mechanisms in human monocytes. J Infect Dis 177:347–354. [PubMed: 9466520]

Pu J, Guardia CM, Keren-Kaplan T, Bonifacino JS (2016) Mechanisms and functions of lysosome positioning. J Cell Sci 129:4329–4339. [PubMed: 27799357]

Qian ZM, Tang PL (1995) Mechanisms of iron uptake by mammalian cells. Biochim Biophys Acta 1269:205–214. [PubMed: 7495872]

Rauen U, Springer A, Weisheit D, Petrat F, Korth HG, de Groot H, Sustmann R (2007) Assessment of chelatable mitochondrial iron by using mitochondrion-selective fluorescent iron indicators with different iron-binding affinities. Chembiochem : a European journal of chemical biology 8:341–352. [PubMed: 17219451]

Russo R, Navarra M, Maiuolo J, Rotiroti D, Bagetta G, Corasaniti MT (2005) 17beta-estradiol protects SH-SY5Y Cells against HIV-1 gp120-induced cell death: evidence for a role of estrogen receptors. Neurotoxicology 26:905–913. [PubMed: 15899520]

Sanchez AB, Kaul M (2017) Neuronal Stress and Injury Caused by HIV-1, cART and Drug Abuse: Converging Contributions to HAND. Brain Sci 7.

Saylor D, Dickens AM, Sacktor N, Haughey N, Slusher B, Pletnikov M, Mankowski JL, Brown A, Volsky DJ, McArthur JC (2016) HIV-associated neurocognitive disorder--pathogenesis and prospects for treatment. Nat Rev Neurol 12:234–248. [PubMed: 26965674]

Scutari R, Alteri C, Perno CF, Svicher V, Aquaro S (2017) The Role of HIV Infection in Neurologic Injury. Brain Sci 7.

Settembre C, Fraldi A, Medina DL, Ballabio A (2013) Signals from the lysosome: a control centre for cellular clearance and energy metabolism. Nat Rev Mol Cell Biol 14:283–296. [PubMed: 23609508]

Shah A, Kumar S, Simon SD, Singh DP, Kumar A (2013) HIV gp120- and methamphetamine-mediated oxidative stress induces astrocyte apoptosis via cytochrome P450 2E1. Cell Death Dis 4:e850. [PubMed: 24113184]

Toggas SM, Masliah E, Mucke L (1996) Prevention of HIV-1 gp120-induced neuronal damage in the central nervous system of transgenic mice by the NMDA receptor antagonist memantine. Brain Res 706:303–307. [PubMed: 8822372]

Turchan J, Pocernich CB, Gairola C, Chauhan A, Schifitto G, Butterfield DA, Buch S, Narayan O, Sinai A, Geiger J, Berger JR, Elford H, Nath A (2003) Oxidative stress in HIV demented patients and protection ex vivo with novel antioxidants. Neurology 60:307–314. [PubMed: 12552050]

Uchiyama A, Kim JS, Kon K, Jaeschke H, Ikejima K, Watanabe S, Lemasters JJ (2008) Translocation of iron from lysosomes into mitochondria is a key event during oxidative stress-induced hepatocellular injury. Hepatology 48:1644–1654. [PubMed: 18846543]

Valentín-Guillama G, López S, Kucheryavykh YV, Chorna NE, Pérez J, Ortiz-Rivera J, Inyushin M, Makarov V, Valentín-Acevedo A, Quinones-Hinojosa A, Boukli N, Kucheryavykh LY (2018) HIV-1 Envelope Protein gp120 Promotes Proliferation and the Activation of Glycolysis in Glioma Cell. In: Cancers (Basel).

Viviani B, Corsini E, Binaglia M, Galli CL, Marinovich M (2001) Reactive oxygen species generated by glia are responsible for neuron death induced by human immunodeficiency virus-glycoprotein 120 in vitro. Neuroscience 107:51–58. [PubMed: 11744246]

Wolff NA, Garrick LM, Zhao L, Garrick MD, Thevenod F (2014) Mitochondria represent another locale for the divalent metal transporter 1 (DMT1). Channels (Austin) 8:458–466. [PubMed: 25483589]

Wolff NA, Garrick MD, Zhao L, Garrick LM, Ghio AJ, Thevenod F (2018) A role for divalent metal transporter (DMT1) in mitochondrial uptake of iron and manganese. Sci Rep 8:211. [PubMed: 29317744]

Xiong J, Zhu MX (2016) Regulation of lysosomal ion homeostasis by channels and transporters. Sci China Life Sci 59:777–791. [PubMed: 27430889]

Yambire KF, Rostosky C, Watanabe T, Pacheu-Grau D, Torres-Odio S, Sanchez-Guerrero A, Senderovich O, Meyron-Holtz EG, Milosevic I, Frahm J, West AP, Raimundo N (2019) Impaired lysosomal acidification triggers iron deficiency and inflammation in vivo. Elife 8.

Dong XP, Cheng X, Mills E, Delling, Wang F, Kurz T, Xu H (2008) The type IV mucolipidosis-associated protein TRPML1 is an endolysosomal iron release channel. Nature 455:992–996. [PubMed: 18794901]

Fernández B, Fdez E, Gómez-Suaga P, Gil F, Molina-Villalba I, Ferrer I, Patel S, Churchill GC, Hilfiker S (2016) Iron overload causes endolysosomal deficits modulated by NAADP-regulated 2-pore channels and RAB7A. In: Autophagy, pp 1487–1506. [PubMed: 27383256]

Liou GY, Storz P (2010) Reactive oxygen species in cancer. Free Radic Res 44:479–496. [PubMed: 20370557]

Lopez SN, Rodriguez-Valentin M, Rivera M, Rodriguez M, Babu M, Cubano LA, Xiong H, Wang G, Kucheryavykh L, Boukli NM (2017) HIV-1 Gp120 clade B/C induces a GRP78 driven cytoprotective mechanism in astrocytoma. Oncotarget 8:68415–68438. [PubMed: 28978127]

Montalbetti N, Simonin A, Dalghi MG, Kovacs G, Hediger MA (2014) Development and Validation of a Fast and Homogeneous Cell-Based Fluorescence Screening Assay for Divalent Metal Transporter 1 (DMT1/SLC11A2) Using the FLIPR Tetra. J Biomol Screen 19:900–908. [PubMed: 24505080]

Russo R, Navarra M, Maiuolo J, Rotiroti D, Bagetta G, Corasaniti MT (2005) 17beta-estradiol protects SH-SY5Y Cells against HIV-1 gp120-induced cell death: evidence for a role of estrogen receptors. Neurotoxicology 26:905–913. [PubMed: 15899520]

Schieber M, Chandel NS (2014) ROS function in redox signaling and oxidative stress. Curr Biol 24:R453–462. [PubMed: 24845678]

Valentín-Guillama G, López S, Kucheryavykh YV, Chorna NE, Pérez J, Ortiz-Rivera J, Inyushin M, Makarov V, Valentín-Acevedo A, Quinones-Hinojosa A, Boukli N, Kucheryavykh LY (2018) HIV-1 Envelope Protein gp120 Promotes Proliferation and the Activation of Glycolysis in Glioma Cell. In: Cancers (Basel).

Viviani B, Corsini E, Binaglia M, Galli CL, Marinovich M (2001) Reactive oxygen species generated by glia are responsible for neuron death induced by human immunodeficiency virus-glycoprotein 120 in vitro. Neuroscience 107:51–58. [PubMed: 11744246]

Yanagawa M, Tsukuba T, Nishioku T, Okamoto Y, Okamoto K, Takii R, Terada Y, Nakayama KI, Kadowaki T, Yamamoto K (2007) Cathepsin E deficiency induces a novel form of lysosomal storage disorder showing the accumulation of lysosomal membrane sialoglycoproteins and the elevation of lysosomal pH in macrophages. J Biol Chem 282:1851–1862. [PubMed: 17095504]

Yang Y, Yao H, Lu Y, Wang C, Buch S (2010) Cocaine potentiates astrocyte toxicity mediated by human immunodeficiency virus (HIV-1) protein gp120. PLoS One 5:e13427. [PubMed: 20976166]

Yoshimori T, Yamamoto A, Moriyama Y, Futai M, Tashiro Y (1991) Bafilomycin A1, a specific inhibitor of vacuolar-type H(+)-ATPase, inhibits acidification and protein degradation in lysosomes of cultured cells. J Biol Chem 266:17707–17712. [PubMed: 1832676]

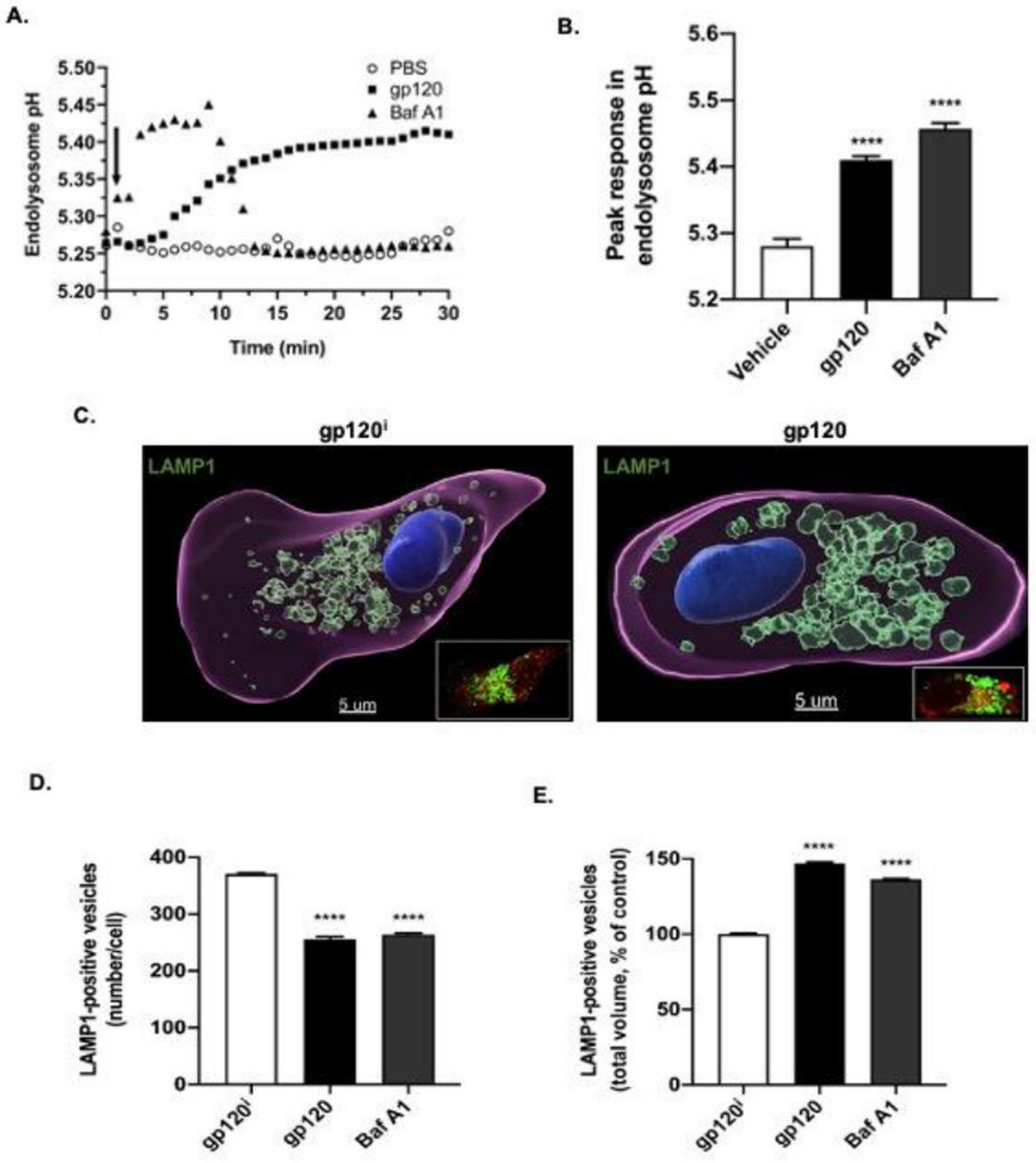

Fig. 1. HIV-1 gp120 increased endolysosome pH and volumes, and decreased endolysosome numbers.

(A) Treatment of U87MG cells with 4 nM HIV-1 gp120 (closed squares) or the vacuolar ATPase inhibitor bafilomycin A1 (Baf A1, 200 nM, closed triangles) de-acidified endolysosomes; de-acidification by HIV-1 gp120 remained elevated for 30 min while the effects of Baf A1 normalized about 12 min following its application. For HIV-1 gp120, peak de-acidification was observed by 30 min whereas for Baf A1 peak de-acidification was observed about 3 min following its application. (B) HIV-1 gp120 significantly increased endolysosome pH units ($p<0.0001$) by 0.13 ± 0.01 pH units from control values of 5.28

± 0.01 to values of 5.41 ± 0.01 and Baf A1 significantly increased endolysosome pH units ($p<0.0001$) by 0.18 ± 0.01 pH units from control values of 5.28 ± 0.01 to 5.46 ± 0.01. n= 90, ****$p<0.0001$. (C) Representative Imaris 9.5 software (Oxford Instruments) reconstructed and laser scanning confocal microscopy (inset) images of U87MG cells treated for 30 min with 4 nM heat-inactivated gp120 (left panel, $gp120^{i}$) or HIV-1 gp120 (right panel). Lysosomes were stained with anti-LAMP1 antibody, plasma membranes were stained with anti-beta1 sodium potassium ATPase antibody (red), and nuclei were stained with anti-DAPI antibody. Qualitatively, endolysosomes exposed to $gp120^{i}$ displayed a perinuclear distribution pattern but were larger and more dispersed towards plasma membranes when exposed to HIV-1 gp120. (D) HIV-1 gp120 and the positive control Baf A1 both significantly ($p<0.0001$) decreased the number of LAMP1-positive vesicles/cell. (E) HIV-1 gp120 and the positive control Baf A1 both significantly ($p<0.0001$) increased the total volume of LAMP1-positive endolysosomes per cell. n= 900, ****$p<0.0001$.

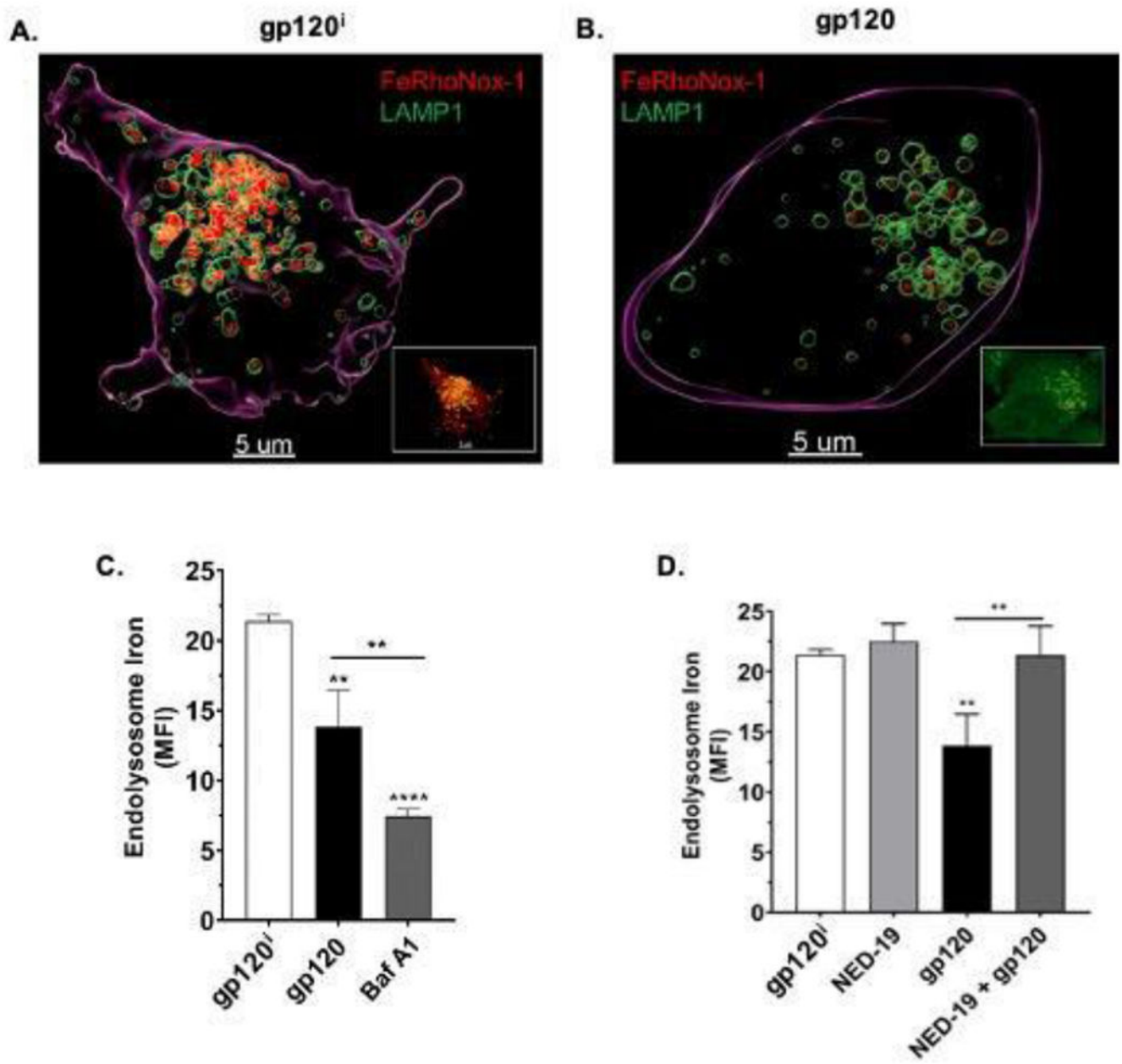

Fig. 2. ***HIV-1 gp120 decreased levels of endolysosome*** Fe^{2+} ***and these decreases were blocked by an inhibitor of two pore channels.***

In U87MG cells, we determined the extent to which heat-inactivated HIV-1 gp120 ($gp120^i$), HIV-1 gp120 (gp120) and bafilomycin A1 (Baf A1) decreased levels of endolysosome Fe^{2+} and whether the inhibitor of two-pore channels Ned-19 blocked these decreases. (A-B) Representative scanning confocal microscope images of U87MG cells treated for 30 min with either (A) heat-inactivated HIV-1 gp120 ($gp120^i$) or (B) 4 nM HIV-1 gp120. Qualitatively, treatment of U87MG cells for 30 min with 4 nM HIV-1 gp120 (Figure 2B) but not $gp120^i$ (Figure 2A) decreased FeRhoNox-1 fluorescence staining for Fe^{2+}. (C) Quantitatively, levels of endolysosome Fe^{2+} as indicated by mean fluorescence units (MFI) for FeRhoNox-1 staining were significantly ($p<0.01$) decreased by HIV-1 gp120 and by

Baf A1 ($p<0.0001$); the decrease produced by Baf A1 was significantly ($p<0.01$) greater than that produced by HIV-1 gp120. (D) Mean fluorescence intensity (MFI) values for FeRhoNox-1 staining were significantly ($p<0.01$) decreased by HIV-1 gp120 and these decreases were effectively blocked by 10 μM Ned-19, an inhibitor of endolysosome two pore channels. N = 900, **$p<0.01$, **$p<0.0001$

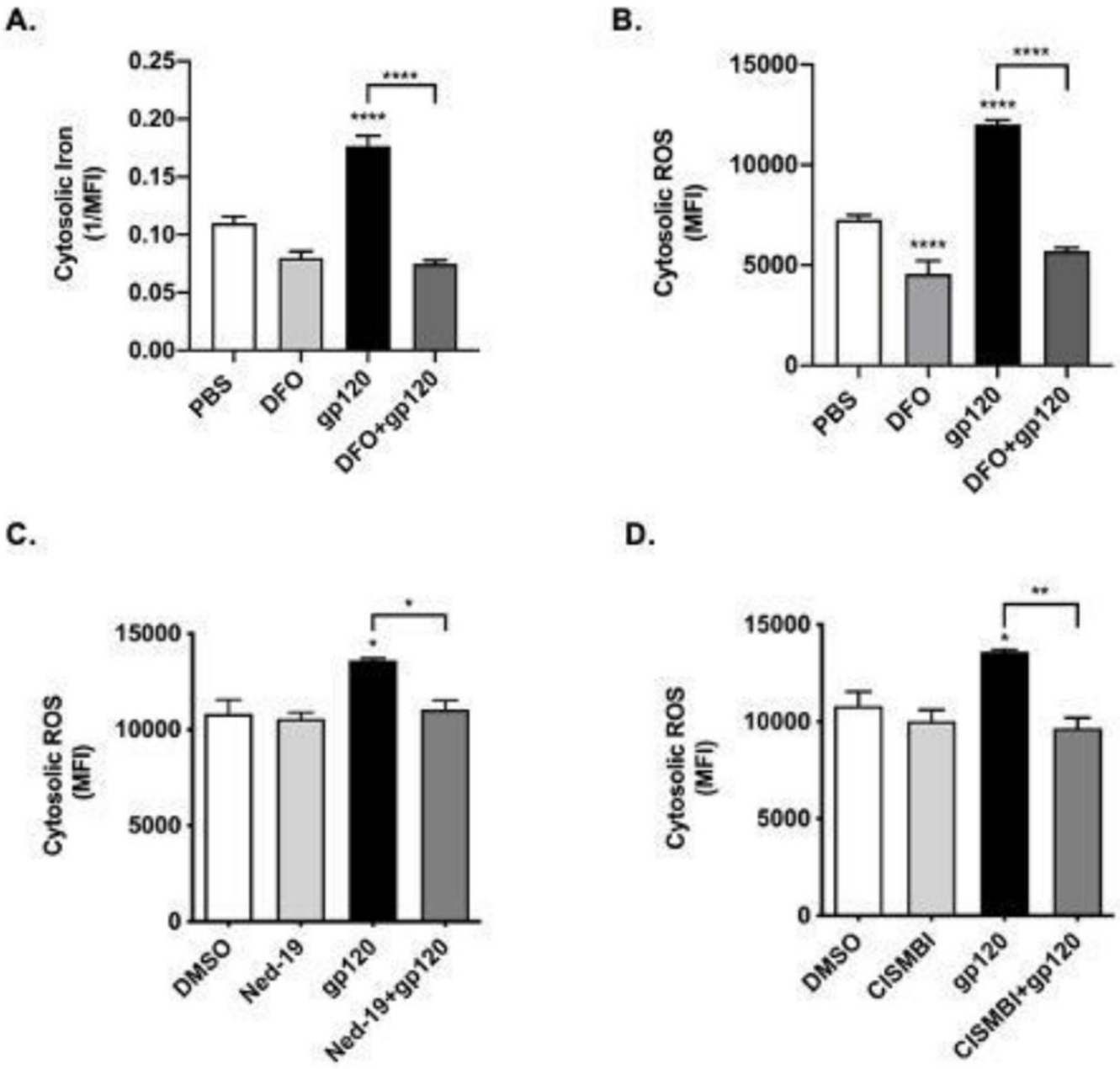

Fig. 3. Effects of deferoxamine, and inhibitors of two pore channels and divalent metal transporter 1 on levels of cytosolic iron and ROS.

(A) Levels of cytosolic Fe^{2+} were measured using the "turn-off" quenching dye PhenGreen SK (PGSK). Data were transformed to the reciprocal of mean fluorescence intensity (1/MFI) to illustrate more clearly the ability of gp120 to increase levels of cytosolic Fe^{2+}. Levels of cytosolic Fe^{2+} were significantly ($p<0.0001$) increased by 30 min treatments with 4 nM HIV-1 gp120. Pre-treatment of cells for 1 h with the endolysosome-specific Fe^{2+} chelator deferoxamine (DFO, 100 μM) significantly ($p<0.0001$) blocked HIV-1 gp120-induced increases in levels of cytosolic Fe^{2+}. Levels of cytosolic Fe^{2+} were not significantly affected by vehicle controls (PBS). (B) Levels of cytosolic ROS using

2,7-dichlorodihydrofluoroscein (DCF) were significantly ($p<0.0001$) increased by 30 min treatments of U87MG cells with 4 nM HIV-1 gp120. Pre-treatment of cells for 1 h with DFO (100 μM) significantly ($p<0.0001$) decreased basal levels of cytosolic ROS and significantly ($p<0.0001$) blocked HIV-1 gp120-induced increases in cytosolic ROS. (C) Pre-treatment of cells with 10 μM Ned-19, an inhibitor of endolysosome associated two pore channels (TPCs), significantly ($p<0.05$) blocked HIV-1 gp120-induced increases in levels of cytosolic ROS. (D) Pre-treatment of cells with 100 μM CISMBI, an inhibitor of divalent metal transporter 1 (DMT1), significantly ($p<0.01$) blocked HIV-1 gp120-induced increases in levels of cytosolic ROS. Levels of DCF fluorescence were measured as mean fluorescence intensity (MFI). N = 10,000, *$p<0.05$; **$p<0.01$; ****$p<0.0001$.

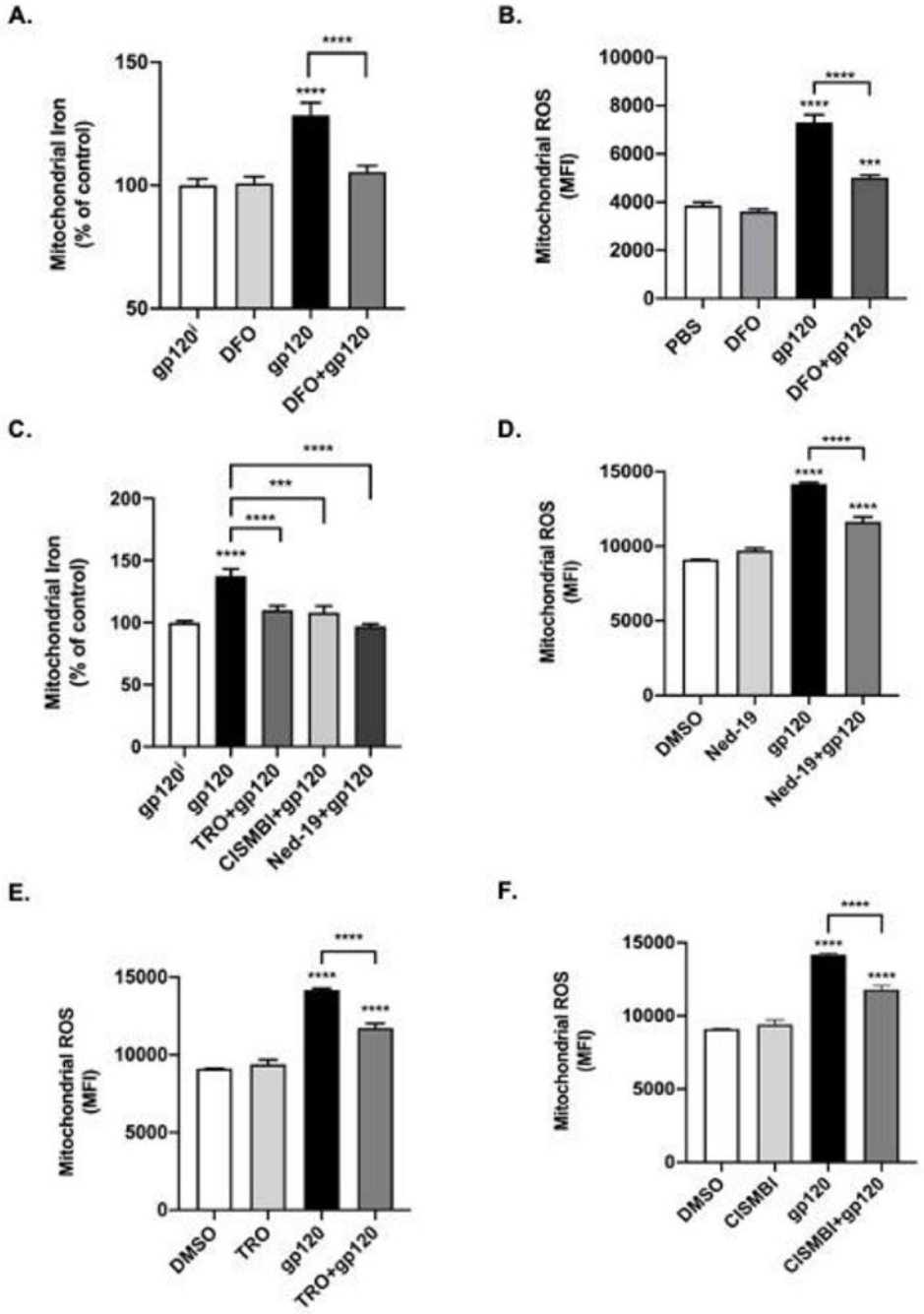

Fig. 4. ***Effects of deferoxamine, and inhibitors of two pore channels, mitochondrial permeability transition pore opening, and divalent metal transporter 1 on HIV-1 gp120-induced increases in mitochondrial*** **Fe^{2+}** ***and ROS levels.***

Mitochondrial iron levels were measured using the quenching dye rhodamine B-[(2,2'-bipyridine-4-yl)-aminocarbonyl]benzyl ester (RDA) and RDA fluorescence data were expressed as 1/MFI to illustrate more clearly the effects of HIV-1 gp120 on levels of mitochondrial iron and ROS. (A) 4 nM HIV-1 gp120 significantly ($p<0.0001$) increased levels of mitochondrial iron while 1 h pre-treatment with 100 μM DFO significantly ($p<0.0001$) blocked HIV-1 gp120-induced increases in mitochondrial Fe^{2+}. (B) MitoSox

Red was used as a measure of mitochondrial ROS and superoxide radicals. Mean fluorescence intensity (MFI) was significantly ($p<0.0001$) increased by 30 min treatment of U87MG cells with 4 nM HIV-1 gp120, while 1 h pretreatment of cells with 100 μM DFO significantly ($p<0.0001$) reduced HIV-1 gp120-induced increases in mitochondrial ROS (C) Pre-treatment of cells with the mitochondrial permeability transition pore inhibitor TRO-19622 (TRO, 3 μM) ($p<0.0001$), the divalent metal transporter 1 inhibitor 2-(3-carbamimidoylsulfanylmethyl-benzyl)- isothiourea (CISMBI, 100 μM) ($p<0.001$), or the two pore channel inhibitor Ned-19 (10 μM, $p<0.0001$) blocked HIV-1 gp120-induced increases in mitochondrial Fe^{2+}. (D) HIV-1 gp120-induced increases in mitochondrial ROS were significantly ($p<0.0001$) inhibited by pretreating cells for 30 min with 10 μM Ned-19, an inhibitor of endolysosome-resident two pore channels. (E) HIV-1 gp120-induced increases in mitochondrial ROS were significantly ($p<0.0001$) inhibited by pretreating cells for 30 min with 3 μM TRO, an inhibitor of mitochondrial permeability transition pore (mPTP) opening. (F) HIV-1 gp120-induced increases in mitochondrial ROS were significantly ($p<0.0001$) inhibited by pretreating cells for 30 min with 100 μM CISMBI, an inhibitor of divalent metal transporter 1 (DMT1). $N \geq 25$, ****$p<0.0001$.

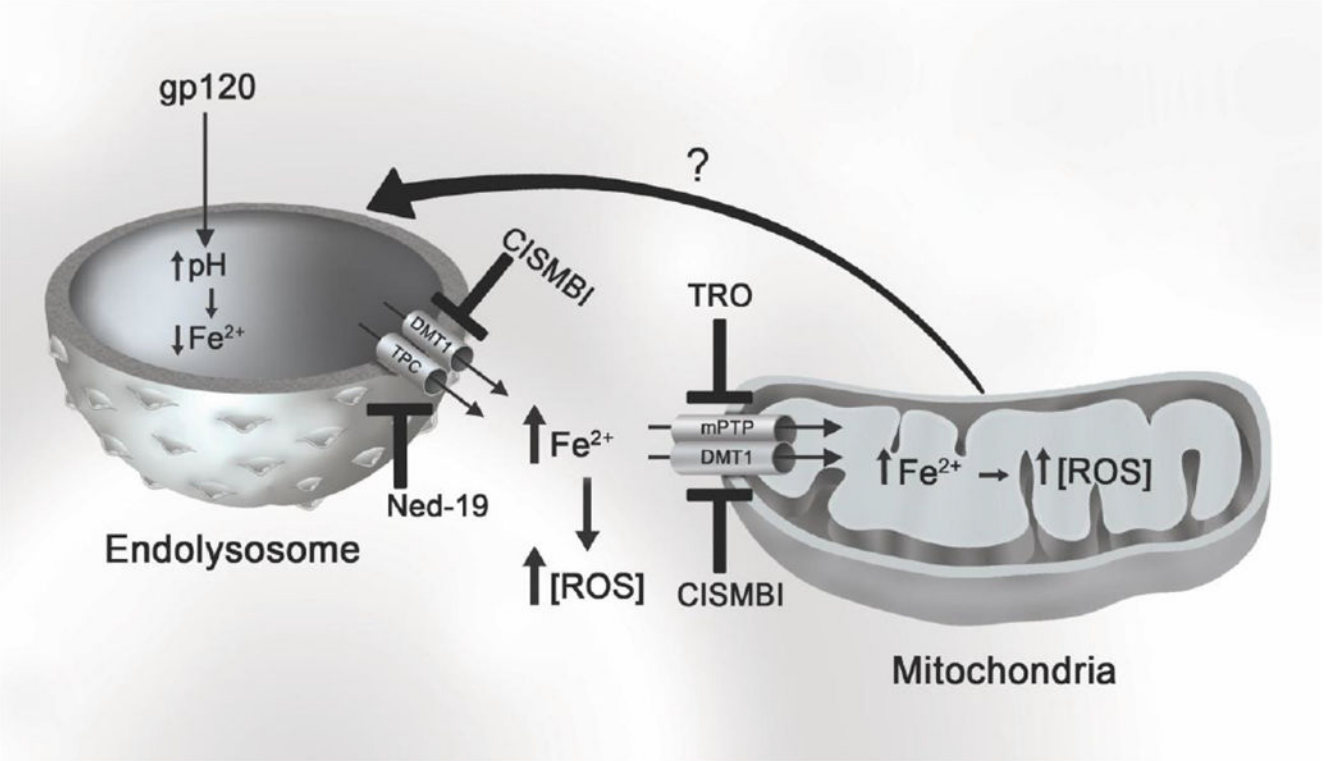

Fig. 5. ***HIV-1 gp120-induced release of*** **Fe^{2+}** ***from endolysosomes results in increased levels of*** **Fe^{2+}** ***and ROS in cytosol and mitochondria.***

HIV-1 gp120 increases endolysosome pH, which then induces an efflux ferrous Fe^{2+} through endolysosome-resident cation channels including divalent metal transporter (DMT1) and two pore channels (TPC). Ferrous iron released from endolysosomes can accumulate in the cytosol and can be uptaken into mitochondria via DMT1 or mitochondrial permeability transition pore (mPTP) opening. Ferrous iron can catalyze Fenton reactions and the generation of reactive oxygen species (ROS). Mitochondrial ROS may signal back to endolysosomes to further exacerbate endolysosome dysfunction and the release of Fe^{2+}. HIV-1 gp120-mediated increases in cytosolic and mitochondrial ROS can be attenuated with inhibitors of DMT1 (CISMBI), TPC (Ned-19), and mPTP (TRO) channels.